Numiform 2001

Implementation of a texture based interpolated yield locus in a FEM code

L. Duchêne, A. M. Habraken & A. Godinas
University of Liège, Liège, Belgium

ABSTRACT: This paper presents a constitutive law based on Taylor's model implemented in our non linear finite element code LAGAMINE. The yield locus is only locally described and a particular interpolation method has been developed. This local yield locus model uses a discrete representation of the material's texture. The interpolation method is presented and a deep-drawing application is simulated in order to show up the influence of the texture evolution during forming processes.

1 STATE OF THE PROBLEM

The objective of our research is to integrate the influence of the material's texture into a finite element code. The constitutive law describing the mechanical behaviour of the studied sample is based on a microscopic approach. The law computation takes place on the crystallographic level. A large number of crystals must be used to represent correctly the global behaviour. The micro-macro transition links the global behaviour to the crystallographic results. The full constraint Taylor's model is used for the computation of the microscopic behaviour of each crystal and for the micro-macro transition. Unfortunately, this model does not lead to a general law with a mathematical formulation of the yield locus. Only one point of the yield locus corresponding to a particular strain rate direction can be computed.

The "direct Taylor's model" assumes that one macroscopic stress results from the average of the microscopic stresses related to each crystal belonging to a set of representative crystals. The computation of the mechanical behaviour involves a large number of crystals and must be repeated for each integration point of the finite element model, for each iteration of each time step. So, such a micro-macro approach consumes large computation time and seems practically not usable.

However, using different simplified approaches, various constitutive laws based on texture analysis have been implemented in the non linear finite element code LAGAMINE. Our first step in the integration of the texture effects has been the use of a 6^{th} order series yield locus defined by a least square fitting on a large number of points (typically 70300) in the deviatoric stress space (see Munhoven et al. 1996). Those points were calculated by Taylor's model based on an assumed constant texture of the material. This fitting is performed once, outside the FEM code. It provides 210 coefficients to describe the whole yield locus. This method, i.e. a global description of the yield locus, is actually used in the FEM code.

Unfortunately, taking into account the texture evolution effects with this yield locus would imply the computation of the 210 coefficients of the 6^{th} order series for each integration point, each time a texture updating is necessary. This would require an impressive amount of computation and memory storage (210 coefficients for each integration point) which is only partially useful as generally the stress state remains in a local zone of the yield locus. So, two new approaches, where the whole yield locus is unknown, have been investigated.

In the first case, some points in the interesting part of the yield locus are computed with Taylor's model. This local zone of the yield locus is then represented by a set of hyperplanes which are planes defined in the five-dimensional deviatoric stress space. These planes being fitted on Taylor's points.

As it has been shown in (Duchêne et al. 1999), the yield locus discontinuities bred by this very simple interpolation method give rise to convergence problems in the finite element code. That is the reason why a second method has been developed.

For that second approach, no yield locus is defined and a direct stress-strain interpolation between Taylor's points is achieved. In this case, the yield stress continuity conditions are fulfilled but, as there is no yield locus formulation, a particular stress integration scheme has to be used.

Both interpolation methods allow us an important

computation time reduction with respect to the "direct Taylor's model" application. Taylor's model is only used to compute some points in order to achieve the interpolation.

These points must be computed in two cases:

- When the current part of the yield locus does not content anymore the new stress state and that a new local zone of the yield locus is required.
- When the plastic strains significantly deform the material and induce changes in the crystallographic orientations, i.e. when the texture evolves. Indeed, the corresponding mechanical behaviour of the material would no more be correctly represented by the old points. A texture updating must take place.

The part yield locus approach presented in this paper can be placed between the microscopic approach (accurate but very slow) and the global yield locus approach (fast but inaccurate and especially not adapted for texture updating).

This paper describes the stress-strain interpolation method; interested readers can refer to (Winters 1996 & Duchêne et al. 1999) for the 6th order and the hyperplanes method. The influence of the texture updating during a forming process has been highlighted by a deep-drawing simulation.

2 STRESS-STRAIN INTERPOLATION

2.1 *Local description of a scaled yield locus.*

The yield locus shape is our present goal. The size of the yield locus is defined by a simple scalar power-type hardening law as already proposed by (Winters 1996). The hereafter proposed method is more an interpolation approach than a local representation of a scaled yield locus. A "function" locally describing the plastic surface is not developed. Nevertheless, this interpolation method assumes the existence of a yield locus.

Let $\mathbf{s}^{*0}$ be one unit stress vector, direction of the central point of the local part of the yield locus that requires an approximation. $\mathbf{s}^{*(i)}$ are five (N) unit stress vectors surrounding $\mathbf{s}^{*0}$ and determining the interpolation domain. They will be called the "domain limit vectors". In practice, the approach has been developed for a N dimensional space but is directly applied to the 5 dimensions case as the goal is to define a local yield locus zone in the deviatoric stress or strain rate space. Hereafter, the notation choice is adapted to the stress space but all the approach can be translated to the strain rate space. When the 6 or (N+1) vectors (5 $\mathbf{s}^{*(i)}$ and 1 $\mathbf{s}^{*0}$) have following properties:

- they are unit vectors:

$$\mathbf{s}^{*(i)}.\mathbf{s}^{*(i)} = 1 \quad \text{(no sum on i) and} \quad \mathbf{s}^{*0}.\mathbf{s}^{*0} = 1 \qquad (1)$$

- there is a common angle between all $\mathbf{s}^{*(i)}$:

$$\mathbf{s}^{*(i)}.\mathbf{s}^{*(j)} = 1+\beta^2(\delta_{ij}-1) \quad \text{with i, j = 1...N} \qquad (2)$$

- there is a common angle between each $\mathbf{s}^{*(i)}$ and $\mathbf{s}^{*0}$:

$$\mathbf{s}^{*0}.\mathbf{s}^{*(i)} = \cos\theta \qquad \text{with i, j = 1...N} \qquad (3)$$

- they determine a regular domain. These choices induce that the central direction $\mathbf{s}^{*0}$ can be computed as a scaled average of the 5 (N) limit vectors $\mathbf{s}^{*(i)}$:

$$\mathbf{s}^{*0} = \frac{1}{\cos\theta}\sum_{i=1}^{N}\mathbf{s}^{*(i)} \qquad (4)$$

The angle θ and the parameter β, both determine the size of the interpolation domain. They are linked by the relation:

$$\beta^2 = \frac{N}{N-1}\sin^2\theta \qquad (5)$$

As the N $\mathbf{s}^{*(i)}$ vectors are linearly independent, they constitute a vector basis of the N-dimensional space. However, as they are not orthogonal, it is interesting to introduce N new vectors with following orthogonal property:

$$\mathbf{ss}^{(i)}.\mathbf{s}^{*(j)} = \delta_{ij} \qquad (6)$$

These vectors are called "contravariant vectors". Equation 6 implies that these vectors are not unit ones and one can check that they depend linearly from vectors $\mathbf{s}^{*(i)}$ and $\mathbf{s}^{*0}$:

$$\mathbf{ss}^{(i)} = \frac{1}{\beta^2}\left(\mathbf{s}^{*(i)} - \frac{1-\beta^2}{\cos\theta}\mathbf{s}^{*0}\right) \qquad (7)$$

The N η-coordinates representing any vector **V** in the $\mathbf{s}^{*(i)}$ vector basis:

$$\mathbf{V} = \sum_{i=1}^{N}\eta_i\mathbf{s}^{*(i)} \qquad (8)$$

are determined thanks to the N $\mathbf{ss}^{(i)}$ vectors:

$$\mathbf{V}.\mathbf{ss}^{(j)} = \sum_{i=1}^{N}\eta_i\mathbf{s}^{*(i)}.\mathbf{ss}^{(j)} = \sum_{i=1}^{N}\eta_i\delta_{ij} = \eta_j \qquad (9)$$

These N η-coordinates are independent to each other, they determine both length and direction of the vector **V**. It is important to note that for a unit vector **V** equal to a domain limit vector $\mathbf{s}^{*(i)}$ the η-coordinates are:

$$\eta_j = \delta_{ij} \qquad \text{with j = 1..5} \qquad (10)$$

The domain limit vectors represent the domain vertices. The N limit boundaries (or edges) of the interpolation domain correspond to one function such that:

$$\eta_i = 0 \tag{11}$$

In fact, the properties associated to isoparametric finite elements are retrieved but extrapolated to N-dimensions. The above choices imply that any point belonging to the interpolation domain is associated to positive η-coordinates.

One convenient way to determine the 5 domain limit vectors $\mathbf{s}^{*(i)}$ is to focus on one particular central direction $\mathbf{s}'^{*0}$ chosen in such a way that its N components are identical. To provide associated domain limit vectors $\mathbf{s}'^{*(i)}$, one computes a linear relation between the central direction and consecutively each vector of the Cartesian basis $\mathbf{e}^{(i)}$:

$$\mathbf{s}'^{*(i)} = \alpha' \mathbf{s}'^{*0} + \beta \mathbf{e}^{(i)} = \underbrace{\alpha' \frac{1}{\sqrt{N}}}_{=\alpha} \begin{pmatrix} 1 \\ 1 \\ 1 \\ 1 \\ 1 \end{pmatrix} + \beta \begin{pmatrix} 0 \\ \vdots \\ 1 \\ \vdots \\ 0 \end{pmatrix} \tag{12}$$

Using the unitary conditions of $\mathbf{s}'^{*(i)}$ and $\mathbf{s}'^{*0}$ and Equation 4, one reaches:

$$\alpha = \frac{\cos\theta}{\sqrt{N}} - \frac{\sin\theta}{\sqrt{N \cdot (N-1)}} \quad \text{and}$$

$$\beta^2 = \frac{N}{N-1} \sin^2\theta \tag{13}$$

Then the rotation linking the real required central point $\mathbf{s}^{*0}$ and the particular one $\mathbf{s}'^{*0}$ is computed by:

$$\mathbf{R} = \mathbf{I} + 2\,\mathbf{s}^{*0} \otimes \mathbf{s}'^{*0} - \frac{\left(\mathbf{s}^{*0} + \mathbf{s}'^{*0}\right) \otimes \left(\mathbf{s}^{*0} + \mathbf{s}'^{*0}\right)}{1 + \mathbf{s}^{*0} . \mathbf{s}'^{*0}} \tag{14}$$

where $\mathbf{I}$ is the second order unit tensor.

This rotation applies $\mathbf{s}'^{*0}$ on the real central vector $\mathbf{s}^{*0}$:

$$\mathbf{R} . \mathbf{s}'^{*0} = \mathbf{s}^{*0} \tag{15}$$

It also provides the domain limit vectors:

$$\mathbf{R} . \mathbf{s}'^{*(i)} = \mathbf{s}^{*(i)} \tag{16}$$

If $\mathbf{s}^{*0}$ and $\mathbf{s}'^{*0}$ are opposite vectors, Equation 14 is not valid; the domain limit vectors $\mathbf{s}^{*(i)}$ can be computed as the opposite of the $\mathbf{s}'^{*(i)}$.

This interpolation domain is called a regular one because the angles between the domain limit vectors are identical (see Equation 2) and the domain limit vectors are unit vectors. However, it is possible to define an interpolated domain based on limit vectors which are non-uniformly located and non-unit vectors as long as they are linearly independent and not parallel to each other. With such non-regular domain, the intrinsic coordinates are still available and require the definition of **ss** vectors (see Equations 6, 8, 9).

The above considerations are sufficient to understand the interpolation approach that has finally been implemented in LAGAMINE code. However, it is interesting to note that further details and properties of such parameterisation of a N dimensional space were further investigated by (Godinas 1998 & Duchêne 2000). They study different interpolation methods on the interpolation domain: linear interpolation in Cartesian coordinates or hyperplane model, linear interpolation in spherical coordinates, approach enriched by bubble mode...

Now, let us consider both 5 dimensional stress and strain rate space. A regular domain is built in the strain rate space, it is defined by its 5 vertices $\mathbf{u}^{*(i)}$ (unit vectors). Thanks to 5 calls to Taylor's module, the associated stress vectors $\mathbf{s}^{(i)}$ can be defined. At this level, no hardening is assumed, that is why we speak here of a scaled yield locus. These 5 stress vectors define a non-regular domain in the stress space. In each space, the concept of contravariant vectors from Equation 6 is applied:

$$\mathbf{uu}^{(i)} . \mathbf{u}^{*(j)} = \delta_{ij} \tag{17}$$

$$\mathbf{ss}'^{(i)} . \mathbf{s}^{(j)} = \delta_{ij} \tag{18}$$

The contravariant vectors $\mathbf{ss}'^{(i)}$ and $\mathbf{ss}^{(i)}$ respectively computed by Equations 18 and 8 differ only because in Equation 8 unit stress directions $\mathbf{s}^{*(i)}$ are used. Here the length of the stress vectors $\mathbf{s}^{(j)}$ is an important characteristic as it defines the yield locus anisotropy. These contravariant vectors $\mathbf{ss}'^{(i)}$ and $\mathbf{uu}^{(i)}$ give in each space, the η-coordinates associated to any stress $\mathbf{s}$ or unit strain rate $\mathbf{u}^*$:

$$\eta_i = \mathbf{uu}^{(i)} . \mathbf{u}^* \tag{19}$$

$$\eta_i = \mathbf{ss}'^{(i)} . \mathbf{s} \tag{20}$$

So any stress vector $\mathbf{s}$ or strain rate direction $\mathbf{u}^*$ can be represented according to the vector basis of their space and the η-coordinates:

$$\mathbf{u}^* = \sum_{i=1}^{5} \eta_i \mathbf{u}^{*(i)} \tag{21}$$

$$\mathbf{s} = \sum_{i=1}^{5} \eta_i \mathbf{s}^{(i)} \tag{22}$$

Physically, one material state corresponds to one stress point and one strain rate direction. In a yield locus formulation, one point on the locus and its normal define both stress and associated strain rate. Here, we work with two interpolation domains and assume that they are physically linked because Taylor's model computes their domain limit vectors.

Due to this close link between the two spaces, it is assumed that the η-coordinates computed by Equations 19 and 20 are equal when physically the stress $\mathbf{s}$ and the strain rate direction $\mathbf{u}^*$ are associated. This property is exactly fulfilled on the domain limit vectors. The stress $\mathbf{s}^{(i)}$ corresponds to the strain rate direction $\mathbf{u}^{*(i)}$ and their η-coordinates are $\eta_i = 1$ and $\eta_j = 0$ ($i \neq j$) in both space. Inside the domain, this property is extended by convenience. It is an assumption. The so-called interpolation approach directly derives from this hypothesis of equality and from Equations 22 and 19. They provide the interpolation relation:

$$\mathbf{s} = \sum_{i=1}^{5} (\mathbf{uu}^{(i)} . \mathbf{u}^*) \mathbf{s}^{(i)} = \mathbf{uu}^{(i)} \otimes \mathbf{s}^{(i)} : \mathbf{u}^* = \mathbf{C} : \mathbf{u}^* \quad (23)$$

For each domain, the $\mathbf{C}$ matrix is computed once from the stress domain limit vectors $\mathbf{s}^{(i)}$ and the contravariant vectors $\mathbf{uu}^{(i)}$ associated to the 5 strain rate vertices $\mathbf{u}^{*(i)}$. Inside one domain, Equation 23 provides the stress state if the strain rate direction is given. The η-coordinates computed by Equation 19 check the domain validity. If values do not belong the interval [0,1], then the interpolation approach of Equation 23 becomes an extrapolation and a new domain is required.

2.2 *Updating of the scaled yield locus description.*

When the available local description of the scaled yield locus does not cover any more the interesting zone, one has to find another local description enclosing the interesting part of the yield locus. Of course the procedure described by Equations 12 to 16 could be repeated using one new strain rate direction $\mathbf{u}^*$ as central point. However, this would provide a new local description forgetting previous information and the discontinuities observed with the hyperplane approach would again appear. Looking at the η-coordinate that does not any more belong to [0,1], one can identify the boundary not respected by the new explored direction. This boundary is identified by N - 1 (= 4) domain limit vectors and can belong to two regular domains. The two neighbour domains defined by their common frontier require only one additional domain limit vector to be completely defined. So only one new vertex must be computed by Taylor's model to identify the neighbour domain that probably contains the new explored strain rate direction. In Lagamine implementation of the interpolation method, the neighbour domain is checked before the computation of a completely new local domain begins.

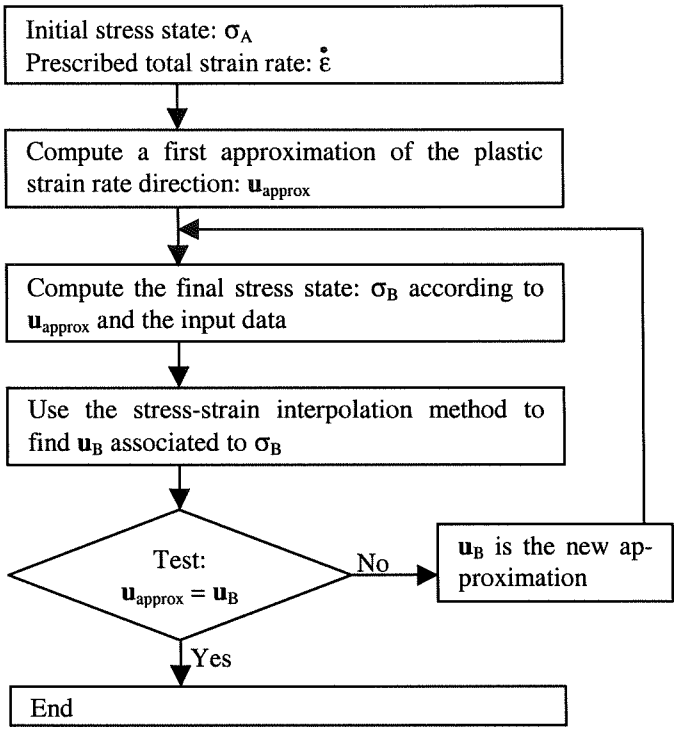

Figure 1. Stress integration scheme.

2.3 *Stress integration scheme*

As already mentioned, the stress-strain interpolation relation (Equation 23) does not use the concept of yield locus in a classical way. So, a specific integration scheme has been developed. The stress integration scheme implemented with our interpolation method is completely different from the classical radial return with elastic predictor; the main ideas are summarised in the diagram of Figure 1 where obviously, no yield locus formulation is used.

As it has been observed during several finite element simulations, this stress integration scheme is well adapted for a local yield locus description and induces a reasonable number of interpolation domain updating.

At this level, the real stress and not the scaled one is aimed, so the size and the shape of the yield locus cannot any more be dissociated. As Equation 23 translates the shape and is assumed to model a reference level of hardening, an additional factor τ is introduced to represent the work hardening:

$$\mathbf{s} = \tau \, \mathbf{C} . \mathbf{u}^* \quad (24)$$

It plays the role of the hardening and is simply linked to the total polycrystal slip Γ by a Swift law:

$$\tau = K(\Gamma_0 + \Gamma)^n \quad (25)$$

As in (Winters 1996), this micro-macro hardening law is identified by a macroscopic uniaxial tensile test.

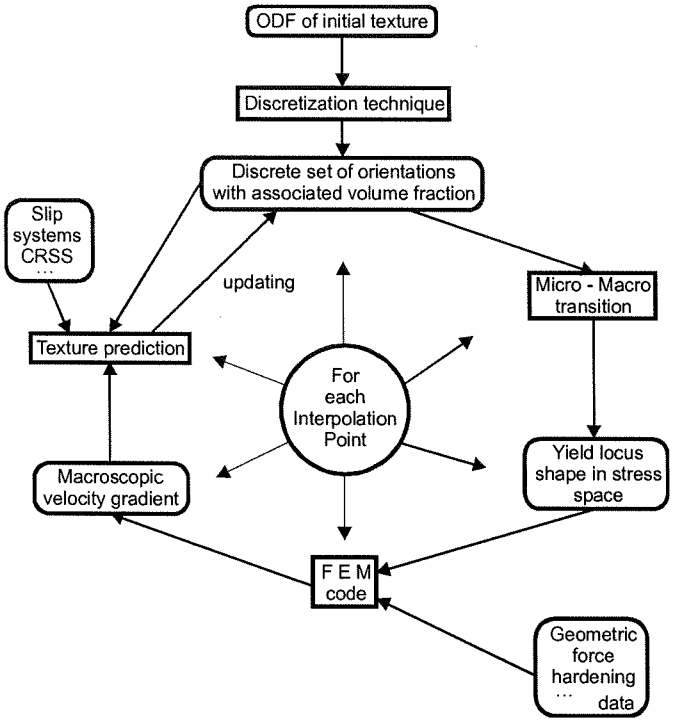

Figure 2. Coupling scheme for texture updating.

2.4 *Implementation of the texture updating*

In this model, not only is the texture used to predict the plastic behaviour of the material, but the strain history of each integration point is taken into account in order to update the texture.

The main ideas of the implementation are summarised in Figure 2. It should be noticed that the constitutive law in the FEM code is based on the interpolation method described earlier and on Taylor's model applied on the actual set of crystallographic orientations through the yield locus. These crystallographic orientations are represented with the help of the Euler angles ranging from 0° to 360° for φ_1 and from 0° to 90° for ϕ and φ_2 so as to take crystal cubic symmetry into account but not the sample symmetry. As shown on Figure 2, the texture updating is achieved outside the main part of the FEM code, for each interpolation point.

During a large finite element simulation, it is not reasonable to achieve a texture updating for each finite element and at the end of each time step. That is the reason why an updating criterion must be used to reduce computation time. This is still under investigation. At this stage, an updating occurs after a predefined number of time steps. A criterion based on a maximum cumulated plastic strain will also be examined.

The lattice rotation of each crystal, inducing the texture updating, is computed with Taylor's model by subtracting the slip induced spin from the rigid body rotation included in the strain history.

3 DEEP-DRAWING SIMULATIONS

In order to show up the influence of the texture evolution during a forming process, a deep-drawing simulation has been examined. Three steels are compared according to their behaviour during the process. The first one is a mild steel, the second one is a dual phase steel and the third one is a complex phase steel. During the calibration of the mechanical properties of these steels which was achieved through tensile tests, extremely different behaviours have been noticed. Their hardening exponents are respectively 0.2186, 0.2238 and 0.1397. Moreover their tensile yield stresses are 136, 293 and 741 N/mm^2 (a factor larger than 5 between them). As we focus on the texture of these steels, their Orientation Distribution Function (ODF) has been measured by X-ray diffraction. The maximum value of this function, i.e. the density of the most represented crystallographic orientation (see Table 1) is an indication of the anisotropy of the studied material.

For this application, the behaviour of the material and particularly its texture have been integrated in the code through a constitutive law based on the 6^{th} order series (see Munhoven et al. 1996 & Winters 1996).

Now, the geometry of the deep-drawing process should be presented. A hemispherical punch with a diameter of 100 mm, a die with a curvature radius of 5 mm and a blankholder are the drawing tools. The drawing ratio is 1.7; the blankholder force is 70 kN; the simulation is achieved up to a drawing depth of 50 mm. This geometry has already been used as the benchmark for the NUMISHEET'99 conference. A Coulomb law is used to model the friction with a coefficient adapted to each steel.

On the finite element mesh, a particular element chosen such that it undergoes completely the drawing process on the curvature of the die is examined. The texture evolution of that element is compared for the three steels. The values of the maximum of the ODF for each steel before and after the process are summarised in Table 1.

Table 1. Maximum value of the ODF during deep-drawing.

Steel	Before deep-drawing	After
Mild steel	6	14.34
Dual phase steel	4.12	6.73
Complex phase steel	6.94	8.52

From Table 1, it can be noticed that the initial anisotropy of the three steels is more or less the same. On the other hand, the behaviour of these steels is quite different during deep-drawing if we focus on the maximum of the ODF (a factor larger than 2 is found at the end of the forming process).

These differences in the steel behaviour can also be pointed out with the use of "r" : the Lankford

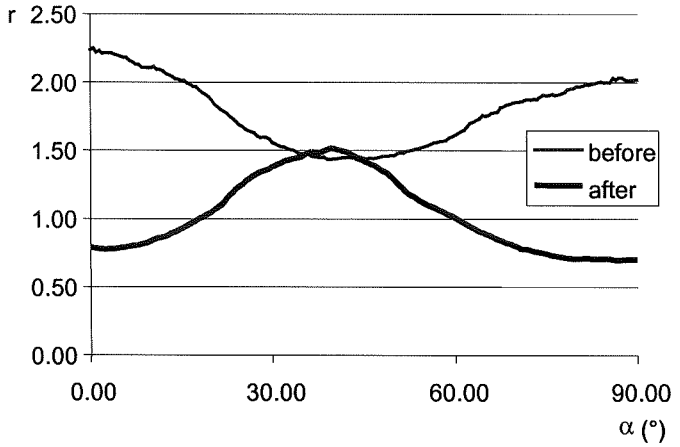

Figure 3. Evolution of the Lankford coefficient for the mild steel before and after deep-drawing (α is the angle from the Rolling Direction).

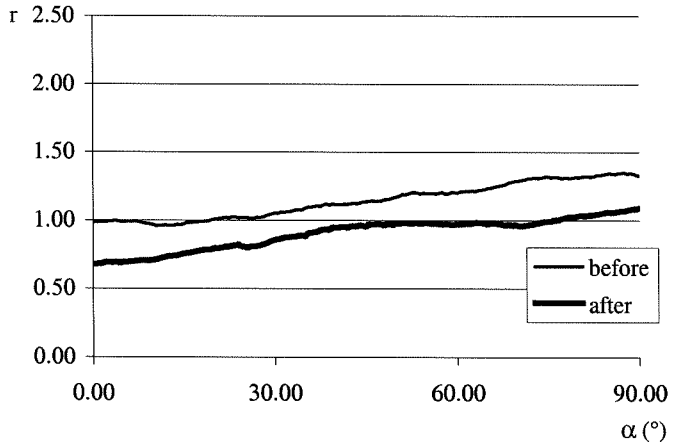

Figure 4. Evolution of r coefficient for the dual phase steel.

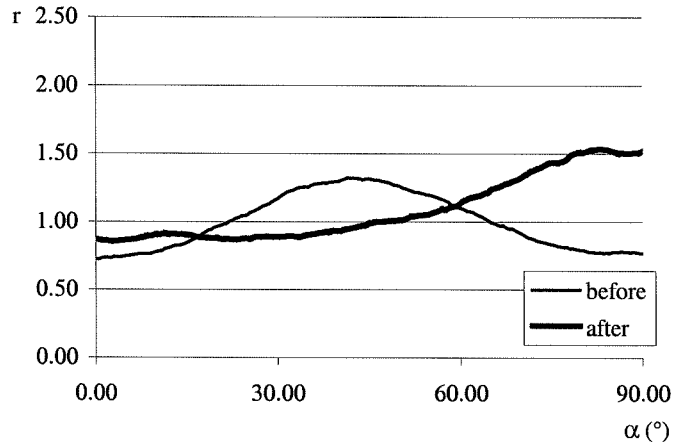

Figure 5. Evolution of r coefficient for the complex phase steel.

coefficients. It is indeed interesting to look at the evolution of the Lankford coefficients during deep-drawing as this parameter is a good indicator for the ability of a steel for deep-drawing (a high value of r allows larger deep-drawing ratios).

Figures 3, 4, 5 show the evolution of the Lankford coefficients during the deep-drawing process. Here again, large differences between the three steels can be noticed. The mild steel is characterised by a high initial r coefficient (inducing a good formability) and a considerable evolution during the simulation. The two other steels have a lower value (around 1.0) and their evolution is also lower. These behaviours are in agreement with the conclusion drawn from the evolution of the maximum of the ODF (see Table 1).

4 CONCLUSIONS

On the deep-drawing application presented here, large texture evolutions have been noticed. Depending on the steel, these evolutions result in modification of the Lankford coefficients. Finally, the behaviour of the steel sheet during a forming process can be quite different from the initial steel characteristics.

As its texture evolution is the most important, the mild steel simulations are used to validate our approach. Different constitutive laws neglecting or not the texture updating are applied and the results will be compared to experimental measurements. This validation step is currently going on.

REFERENCES

Duchêne, L. 2000. *Implementation of a yield locus interpolation method in the finite element code LAGAMINE.* DEA Graduation Work, Ulg, Liège.

Duchêne, L., Godinas, A. & Habraken, A. M. 1999. Metal plastic behaviour linked to texture analysis and FEM method. *Proc. 4th Int. Conf.: NUMISHEET'99.*

Godinas, A. 1998. Définition locale du comportement plastique d'un matériau. *Convention RW n°2748, intermediate report n°27.*

Munhoven, S., Habraken, A. M., Van Bael, A. & Winters, J. 1996. Anisotropic finite element analysis based on texture. *Proc. 3rd Int. Conf.: NUMISHEET'96*: 112-119.

Winters, J. 1996. *Implementation of Texture-Based Yield Locus into an Elastoplastic Finite Element Code.* Ph. D. Thesis, KUL, Leuven.